Laboratory Tests of a New Multi-frequency Coherent Doppler Profiler in Oscillatory Flow Boundary Layers

A.E. Hay[1] and L. Zedel[2]

[1]Department of Oceanography, Dalhousie University, Halifax, NS, Canada; PH (902) 494-6657; email: alex.hay@dal.ca

[2]Department of Physics and Physical Oceanography, Memorial University, St. John's, NL, Canada; PH (709) 737-3106; email: zedel@mun.ca

ABSTRACT

The last two decades have witnessed increasing use of acoustic remote sensing technologies for sediment dynamics measurements in aqueous environments. The approach is driven by the need to minimize disturbances to the fluid-sediment interactions occurring at or close to the mobile bed. This requirement is especially critical in wave-dominated environments, since the wave bottom boundary layer is typically O(10) cm thick, and thus inaccessible to invasive measurement methods during active transport conditions. Motivated in part by the need to measure turbulent fluxes, and thus to obtain simultaneous, collocated measurements of suspended particle concentration and velocity, we have developed a multi-frequency coherent Doppler profiler capable of resolving the vertical structure of the wave bottom boundary layer on both wave period and turbulent time scales. Results are presented from laboratory experiments with this new system in oscillatory flow boundary layers over both fixed roughness and evolving sand ripples.

INTRODUCTION

Previous advances in acoustic profiling techniques have tended to focus either on velocity measurements using a single acoustic frequency, or on suspended sediment concentration and size measurements using multiple frequencies (the latter being required to resolve the size-concentration ambiguity in the backscatter amplitude at a single frequency). We have developed a new Doppler profiling system which makes use of broadband transducer and advanced digital signal processing technologies to operate at up to 4 different frequencies simultaneously. Our motivation for implementing simultaneous operation at multiple frequencies was two-fold: (1) to use the frequency-dependence of the rate of change of phase in a coherent pulse sequence to resolve velocity ambiguities automatically; (2) to use the frequency-dependence of the backscattered signal amplitude to resolve the scatterer size/concentration ambiguity when inverting the backscatter intensity to suspended sediment concentration. The details of the MFDop system are outlined in Hay et al. (2008). In this paper we present results obtained with this new system in a series of oscillatory boundary layer experiments carried out in the laboratory. The purpose of these experiments was to test the ability of the new instrument to resolve the vertical structure of turbulent oscillatory boundary layers, over both fixed roughness and mobile beds, and of both mean and turbulent quantities, at scales comparable to those that can be expected in wave-dominated environments in the field.

33rd IAHR Congress: Water Engineering for a Sustainable Environment

ISBN: 978-94-90365-01-1

METHODS

The measurements were made with the short-range version of the MFDop, for which the beam intersection point is 40 cm from the centre transducer. Profile acquisition rates were ca. 100 Hz, with 3mm range resolution. Transmit frequencies were 1.2, 1.5, 1.8, and 2.1 MHz: The velocity results presented here are based on the 1.2 and 1.8 MHz data. Horizontal and vertical velocities are designated by u and w respectively. Turbulent velocities u' and w' were determined by high-pass filtering the u and w time series using a 5th-order Butterworth filter with a 0.5 Hz cutoff frequency.

The oscillatory boundary layer experiments were carried out in the Ripple Kart facility at Dalhousie: a 7 m long, 0.9 m wide tank with a wheeled "Kart" riding on rails mounted atop the tank side walls. A 2 m long, 0.8 m wide, flat bed is suspended from the Kart at a depth below the water surface of ca. 0.5 m. The water depth is 0.7 m. The Kart is driven by a Scotch yoke mechanism. The oscillation period, T_p, is 10 s. The oscillation excursion, d, is adjustable. Experiments were carried out with two fixed grain roughness beds: a fine-grained sand paper ("no-skid"); and ca. 1 cm sized crushed gravel glued in place. Mobile bed experiments were carried out with 200 μm median diameter (D_{50}) sand, from an initially flattened bed. The sand bed was ca. 10 cm thick.

Data were collected in individual runs, each approximately 15 cycles (150 s) in duration. Phase-averaged results were computed for each run relative to a 10 s period sinusoid fitted to the Kart velocity as measured by the MFDop. Full period and half-cycle averaged vertical profiles of the various quantities of interest were obtained either as a function of range from the centre transducer, or as a function of height above the bed. For the latter, range to the bed was determined from the backscatter intensity on a low-gain output from the centre transducer using the intensity-weighted average range within the range interval containing the bottom echo.

In the mobile bed experiments, bed elevation profiles were measured using laser light sheets and a digital camera with mm accuracy, following a procedure similar to that described by Crawford and Hay (1998). The photographs were taken with a Nikon D80 digital camera, using three laser light sheets $\sim$5 cm apart, at 5 oscillation cycle intervals. The bed elevation measurements were made in a separate experiment: i.e. not during the MFDop runs, but with the same configuration (same sand, same d).

RESULTS

a. Fixed Grain Roughness

Phase-averaged horizontal velocities in the frame of reference moving with the Kart are shown in Figure 1 as a function of oscillation phase near Kart reversal at 180°. Panel **a** shows the results for the low roughness (no-skid) surface and $d = 90$ cm. There is very little, if any, indication of an oscillatory boundary layer. Panel **b** shows the same information from the high roughness (gravel) surface and a higher excursion. In the latter case, the oscillatory boundary layer is clearly evident, exhibiting a phase lead which extends to ca. 5 cm above the bed, and which reaches a value of $\sim$15° close to the bed.

The horizontal velocity can be written in the form

$$u = u(z)\exp\left[i(\omega t + \phi(z))\right] \tag{1}$$

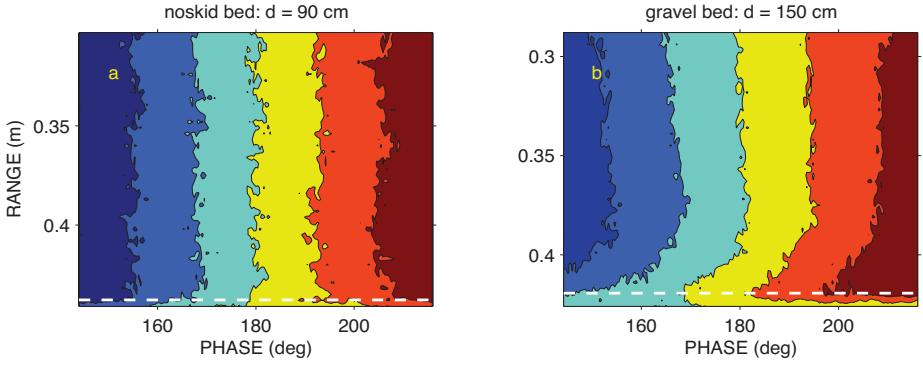

Figure 1: Phase-averaged horizontal velocity above fixed roughness beds: (a) no-skid surface, $d = 90$ cm; (b) gravel surface, $d = 150$ cm. Phases of 0° and 180° correspond to the zero-crossings in the RippleKart velocity. Dashed white lines indicate range at which contamination by the bottom echo first appears. Contour intervals are: (a) 6 cm/s; (b) 11.5 cm/s.

Figure 2 shows the vertical profiles of $u(z)/u_{bo}$ (u_{bo} being the Kart velocity amplitude) and $\phi(z)$ for the no-skid and gravel surfaces at two different excursions. The boundary layer clearly becomes more pronounced with increasing excursion amplitude and increasing bed roughness. Note especially the appearance of the velocity overshoot for the gravel surface at $d = 150$ cm, a well-known characteristic of turbulent oscillatory boundary layers. There are two important additional points. (1) Within about 1 cm of the bed, the phase lead stops increasing continuously toward the bottom and in some cases even starts to decrease (Figure 2d). This effect is due to contamination of the near-bottom bins by the high amplitude bottom return. Thus, the velocities and phases within this 1 cm thick zone are not accurate. (2) Far from the bed, at ca. 10 cm heights, $|u(z)|/u_{bo}$ does not tend to unity as expected, but to a value which is greater than one and becomes increasingly so as the excursion and bed roughness increase. This effect is due to the reaction flow that develops in the tank in response to the volume of water displaced by the moving tray. In the frame of reference moving with the Kart, this flow is in phase with u_b.

b. Mobile Bed

Profiles of bed elevation, η, during the ripple development from an initially flat bed are shown in Figure 3a. These profiles are from one of the three laser light sheets. The corresponding values of the RMS bed elevation σ_η, are plotted in Figure 3b. The error bars represent ± one standard deviation, determined from the profiles for each of the three light sheets.

As Figure 3 indicates, the bed remained essentially flat for the first few minutes, then low amplitude, 5 to 7 cm wavelength ripples developed quite rapidly, maintaining relatively constant amplitude and wavelength while steadily migrating to the right. These ripples were very 2-dimensional, as indicated by the small error bars. Shortly after 10 minutes, the mean ripple amplitude underwent a sharp increase, accompanied by an increase in the variance among the profiles (indicated by the increased length of the error bars). These increases are caused by coalescence of the 5 to 7 cm wavelength ripples into larger scale, increasingly 3-dimensional ripples.

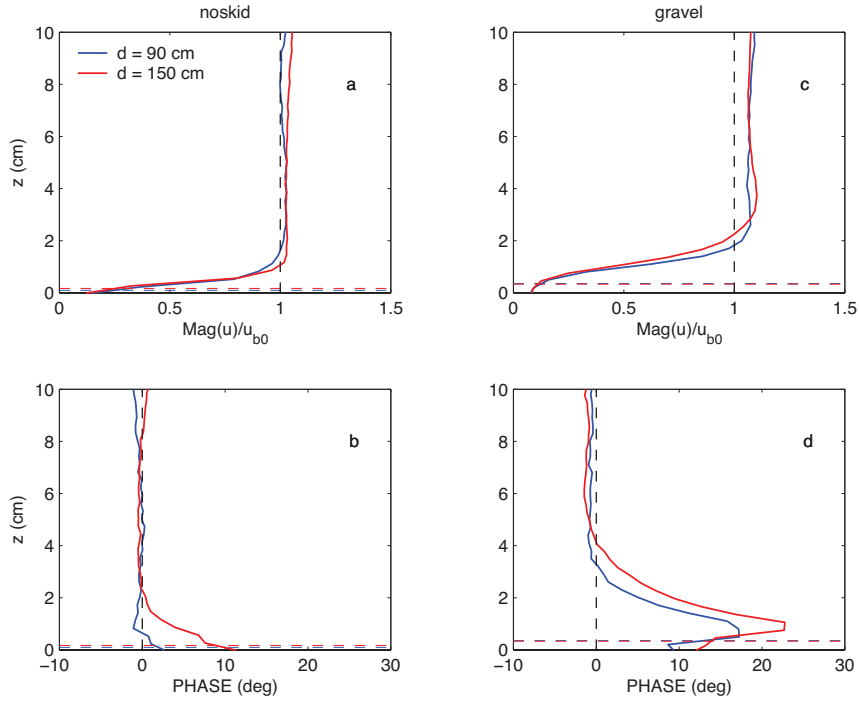

Figure 2: Vertical profiles of $|u|/u_{bo}$ and phase for: (a) and (b) no-skid surface; (c) and (d) fixed gravel surface.

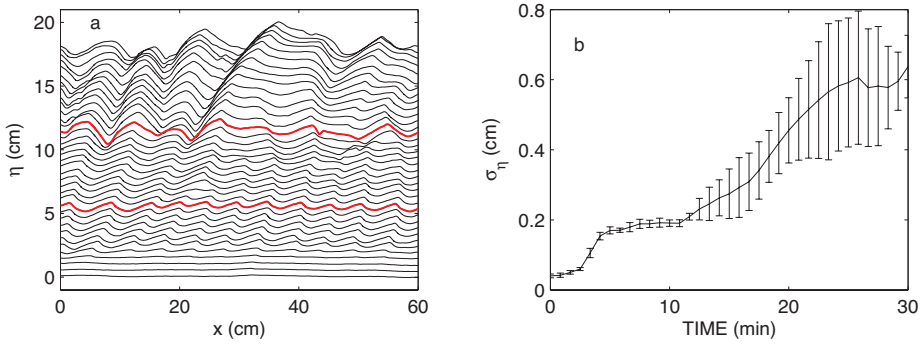

Figure 3: (a) Bed elevation profiles, one every 5 oscillations. Red indicates the profiles at 10 and 20 min. (b) RMS roughness, σ_η, vs time.

Profiles of $|u|/u_{bo}$, phase ϕ, RMS turbulent velocity fluctuations u'_{rms}, w'_{rms}, and turbulent Reynolds stress $-\langle u'w'\rangle$, are shown in Figure 4 for elapsed times of 10 and 39 min. Note the phase lead near the bed, and the thickening of the boundary layer as the ripple amplitude increased. Note also that, far from the bed, $|u|/u_{bo} > 1$, as in the fixed roughness runs, but more pronounced. This larger departure from unity is due to the thickness of the mobile sediment bed, which induces a stronger reaction flow in the tank. Note the horizontal

dashed lines indicating the maximum height relative to mean bed level of the bed elevation features passing under the MFDop or, equivalently, corresponding to the minimum range to the bed during the oscillation cycle.) The RMS turbulence levels (Figure 4c) peak at heights 0.5 to 1 cm above these dashed lines, as do the Reynolds stresses (Figure 4d).

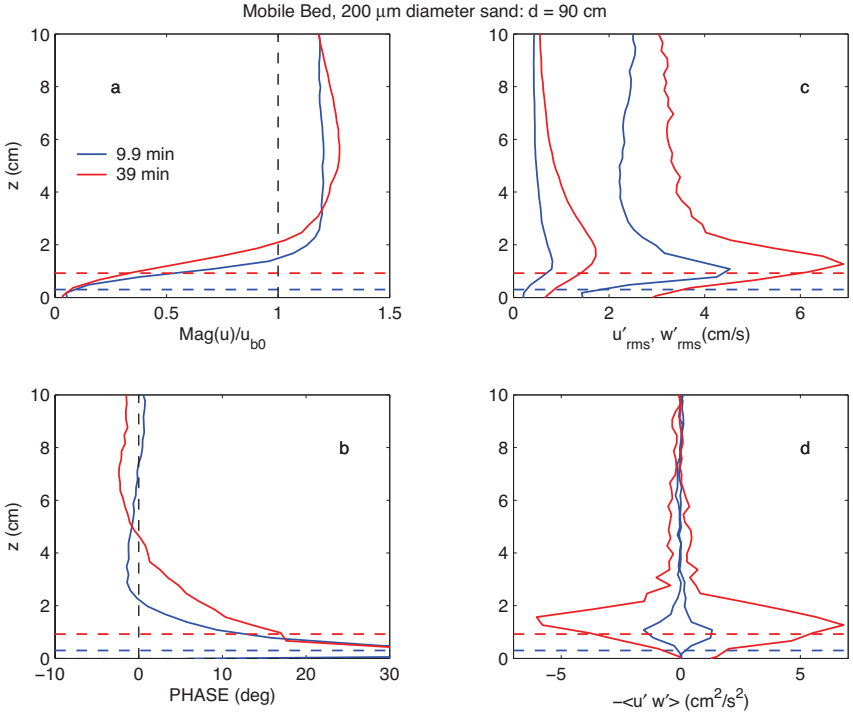

Figure 4: Mobile bed, $d = 90$ cm. Vertical profiles after 10 min (blue) and 39 min(red) of: (a) $|u|/u_{bo}$; (b) phase; (c) RMS turbulent velocity fluctuations; and (d) Reynolds stress, averaged over each half-cycle.

The height of the near-bed peak in the half-cycle mean Reynolds stress profile was selected as an objectively determinable height at which to trace the development near bed phases and turbulence quantities as the bed evolved without undue contamination of these signals from the bottom echo. Figure 5 shows the resulting time histories of u'_{rms}, w'_{rms}, phase, and $-\langle u'w'\rangle$ at this height. The turbulent velocity fluctuations increase gradually with time, and tend to plateau after 25 min. (Note that at short times, when turbulence levels are low, $u'_{rms} \sim 5w'_{rms}$. This difference is due to the bistatic beam geometry of the MFDop, which results in a noise floor for u much greater than that for w.) The phases are scattered, but remain roughly constant on average after the first 5 min, varying between about 10° and 30°. These values are consistent with previous laboratory measurements of the phase lead in turbulent oscillatory boundary layers [Jensen et al. (1989), Sleath (1987), Van Doorn (1982)]. The Reynolds stresses increase with time.

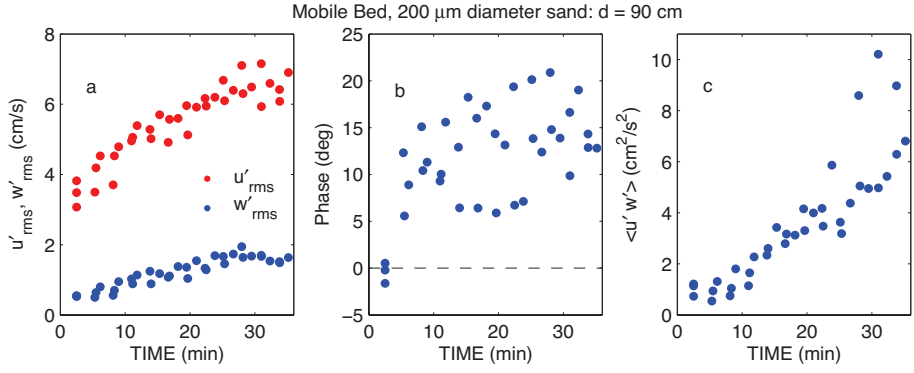

Figure 5: Mobile bed, $d = 90$ cm. Time evolution at the height of maximum mean Reynolds stress of: (a) RMS turbulent velocity fluctuations; (b) phase; and (c) maximum mean Reynolds stress.

Nielsen (1992)

Friction velocities, u_*, were computed using

$$u_* = -2\langle u'w' \rangle \tag{2}$$

where the factor of 2 is used to estimate the maximum stress from the $\langle\ \rangle$ half-cycle average. The resulting values are plotted in Figure 6a, and exhibit a roughly linear increase with time, as indicated by the best-fit straight line. The wave friction factor, f_w, given by

$$u_*^2 = \frac{f_w}{2} u_b^2, \tag{3}$$

was also computed and is shown in Figure 6b. In Equation (3), u_b was set equal to $|u(z)|$ averaged over the top three bins in the profile, and so includes the contribution of the reaction flow to the relative motion of Kart and water far from the sediment surface. Also shown in Figure 6b are the expected values of f_w based on

$$f_w = 2/\sqrt{Re} \tag{4}$$

and

$$f_w = \exp\left[5.213\left(\frac{r}{A}\right)^{0.194} - 5.977\right], \tag{5}$$

where r is the hydraulic roughness of the bed. The value given by Equation (4) is indicated by the dashed red line in Figure 6b, and applies if the wave Reynolds number, Re, is less than 3×10^5 (Nielsen, 1992, p. 24). The oscillation Reynolds number is given by

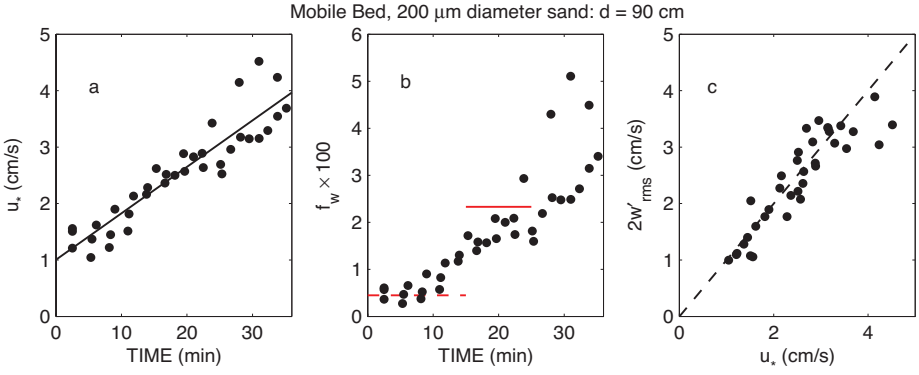

Figure 6: Mobile bed, $d = 90$ cm. Time evolution of: (a) u_* and (b) f_w. The solid line in (a) is the best fit straight line. The dashed and solid red lines in (b) are the expected values based on Equations (4) and (5), respectively. Panel (c) shows $2w'_{rms}$ vs u_*. The dashed line is the 1:1 line (i.e. not a fit).

$$Re = A^2\omega/\nu, \tag{6}$$

where ν is the kinematic viscosity, and A is the semi-excursion. With $A = u_o\omega$ and $T_p = 10$s, $Re = 1.8 \times 10^5$.

The prediction from Equation (5), which is Swart's empirical relationship for f_w, is indicated by the solid red line and was computed using

$$r = 8\eta_o(\eta_o/\lambda), \tag{7}$$

the empirical relationship given by Nielsen (1992, p. 155) for the hydraulic roughness of wave-generated ripples. The value of r was computed using $\eta_o = 2\sqrt{2}\sigma_\eta$ for the ripple height, $\sigma_\eta = 0.3$ cm (Figure 3b), and 0.1 for the ripple steepness, η_o/λ (Figure 3a). Nielsen included a second term in Equation (7) to account for the contribution of moving sand grains. This additional term involves the grain roughness Shields parameter $\theta_{2.5}$, which is 0.12 here. Nielsen's second term has two forms, one for wave energy dissipation estimates and one for sediment transport estimates. The dissipation form yields a value of 0.009, a 40% increase in the value indicated by the solid red line. The sediment transport form yields 1×10^{-4}, which is negligible here.

Finally, the observed values of u_* are compared to $2w'_{rms}$ (evaluated at the height of maximum Reynolds stress) in Figure 6c. The use of $2w'_{rms}$ as a proxy estimate of u_* has been indicated in a number of laboratory experiments (see Nielsen 1992, p. 79), and we have used it to obtain estimates of f_w from measurements of w'_{rms} in the field [Smyth et al. (2002), Smyth and Hay (2002), Smyth and Hay (2003), Newgard and Hay (2007)]. Figure 6c provides additional support for this proxy estimate of u_*.

CONCLUSIONS

The results from these laboratory experiments indicate that the multi-frequency Doppler system is able to resolve the vertical structure of mean and

turbulent quantities through the oscillatory boundary layer to within about 1 cm of the mean bed level, for both fixed roughness and rippled mobile beds. The 1-cm contamination zone is due to the combined effects of beam divergence and non-causal digital filters in the data acquisition system, and improvements are possible in both cases. We regard as particularly promising the near-bed Reynolds stresses and the associated positive comparisons between the wave friction factors derived from the measured stresses and the predictions of existing empirical formulae. The vertical structure of the orbital velocity magnitude and phase are also promising, at least qualitatively.

Further developments of the system in the near future will include: (1) the implementation of multi-frequency inverses to obtain suspended sediment concentration and size measurements and, in particular, suspended sediment fluxes; and (2) a nearshore field experiment.

ACKNOWLEDGEMENTS

We thank Wesley Paul and Robert Craig for their work on the MFDop hardware and software, and Richard Cheel for assisting with the laboratory experiments including processing the laser light sheet photographs and various important refinements to the RippleKart facility. This research was funded by the Coastal Geosciences Program of the U.S. Office of Naval Research and the Natural Sciences and Engineering Research Council of Canada.

REFERENCES

Crawford, A. M. and A. E. Hay (1998). "A simple system for laser-illuminated video imaging of sediment suspension and bed topography." *IEEE J. Oceanic. Eng.*, 23(1), 12-19.

Hay, A.E., L. Zedel, R. Craig, and W. Paul (2008). "Multi-frequency, pulse-to-pulse coherent Doppler sonar profiler." In *Proceedings of the IEEE/OES/CMTC Ninth Working Conference on Current Measurement Technology*, 25-29

Jensen, B. L., B. M. Sumer, and J. Fredsoe (1989). "Turbulent oscillatory boundary layers at high Reynolds numbers." *J. Fluid Mech.*, 116, 265-298.

Newgard, J. P., and A. E. Hay (2007). "Turbulence intensity in the wave boundary layer and bottom friction under (mainly) flat bed conditions." *J. Geophys. Res.*, C09024,doi:10.1029/2006JC003881.

Nielsen, P. (1992). "Coastal Bottom Boundary Layers and Sediment Transport." World Scientific, River Edge, New Jersey, 324 pp.

Sleath, J. F. A. (1987). "Turbulent oscillatory flow over rough beds." *J. Fluid Mech.*, 182, 369-409.

Smyth, C., A.E. Hay, and L. Zedel (2002). "Coherent Doppler profiler measurements of near-bed suspended sediment fluxes and the influence of bedforms." *J. Geophys. Res.*, 107, C8, 19.1-19.20.

Smyth, C. and A. E. Hay (2002). "Wave friction factors in nearshore sands." *J. Phys. Oceanogr.*, 32(12), 3490-3498.

Smyth, C. and A. E. Hay (2003). "Near-bed turbulence and bottom friction during SandyDuck97." *J. Geophys. Res.*, 108(C6), 10.1029/2001JC000952.

Van Doorn, T. (1982). "Experimenteel onderzoek naar het snelheidsveld in de turbulente bodemgrenslaag in een oscillerende stroming in een golftunnel." *Delft Hydraulics Laboratory Rep. M1562-1b*, Delft, Netherlands.